Transcriptome profiling of the ventral pallidum reveals a role for pallido-thalamic neurons in cocaine reward

Michel Engeln[1,2,#], Megan E. Fox[1,3], Ramesh Chandra[1], Eric Y. Choi[1], Hyungwoo Nam[1], Houman Qadir[1], Shavin S. Thomas[1], Victoria M. Rhodes[1], Makeda D. Turner[1], Rae J. Herman[1], Cali A. Calarco[1], Mary Kay Lobo[1#].

1. Department of Anatomy and Neurobiology, University of Maryland School of Medicine, Baltimore, MD, USA.

2. University of Bordeaux, CNRS, IMN, UMR 5293, F-33000 Bordeaux, France.

3. Department of Anesthesiology & Perioperative Medicine, Penn State College of Medicine, Hershey, PA, USA.

Address Correspondence to

Mary Kay Lobo
20 Penn St
HSFII Building, Rm 265
Baltimore, MD 21201
USA
Tel: +1 410-706-8824
Email: mklobo@som.umaryland.edu
ORCID : 0000-0002-9419-2079

Or

Michel Engeln
Institut des Maladies Neurodégénératives - UMR 5293
146 rue Léo Saignat
Zone Nord - Bat 1A - 3e étage
33076 Bordeaux cedex
France
Tel: +33 055-757-1554
Email: michel.engeln@u-bordeaux.fr
ORCID: 0000-0003-3970-7022

Funding: This work was funded by NIH grants R01MH106500, R01DA038613, R01DA047843 and Israel-US Binational Science Foundation 201725 (to MKL), K99DA050575 (to MEF), F31DA052967 (to EC), T32DK098107 and F32DA052966 (to CAC).

Conflict of Interest: The authors declare they have no conflicts of interest.

Abstract

Psychostimulant exposure alters the activity of ventral pallidum (VP) projection-neurons. However, the molecular underpinnings of these circuit dysfunctions are unclear. Using RNA-sequencing followed by circuit-specific gene expression assays, we revealed a key role for the VP to mediodorsal thalamus (VP-MDT) projection neurons in cocaine-related behaviors in mice. Our analyses demonstrated that the transcription factor Nr4a1 bidirectionally modulated dendritic spine dynamics in VP-MDT neurons and positively regulated pathological drug use.

Main text

Originally associated with motor functions, the ventral pallidum (VP) has gained attention for its role in motivation and reward-seeking behaviors [1-5]. Studies dissecting the precise role of the VP in reward revealed a heterogenous brain region composed of diverse cell subtypes and sub-circuits[1, 6, 7]. VP neurons have different roles in reward processing based on their cellular identity (e.g., glutamateric vs. GABAergic, the expression of calbindin vs. parvalbumin, etc.) or output structure [1, 3, 6, 8], and undergo specific plastic changes following drug exposure [2, 7]. While a growing number of studies show changes in neuronal activity following drug exposure, data about molecular adaptations supporting these plastic changes in the VP is lacking.

To characterize these molecular alterations, we trained mice to self-administer cocaine (or saline) for 10 days (**Figure 1a**). Ventral pallidum tissue was collected 24h following the last drug-intake session and processed for RNA sequencing. We found 363 significantly differentially expressed (SDE) genes in mice taking cocaine with relatively similar proportions of up- and down-regulated genes (46.8% vs. 53.2% respectively; **Figure 1b; Supplementary Table 1**). We

performed Gene Ontology (GO) analysis on this subset of genes and found significant changes in multiple neuronal morphology-related GO terms at the 'Biological', 'Cellular' and 'Molecular' levels (**Figure 1c**). Interestingly, at the "Cellular Component" level, neuronal morphology-related terms comprised 40.6% of all GO terms. This represented 200 unique genes, which constituted 55% of all the SDE genes. Multiple significant GO terms referred to structural plasticity and dendritic spines, consistent with described drug-induced changes in neuronal activity [1, 3, 7].

We then investigated the potential transcriptional mechanisms underlying these changes in structural plasticity. We ran a transcriptional regulation analysis on the significant "Cellular Component" GO terms and found that *Nr4a1* (Nuclear receptor subfamily 4, group A, member 1, or *Nur77*) showed direct motif similarity with 19.1% of the genes from 'Neuron projection', 19% of the genes from 'Postsynaptic membrane' and 16.1% of the genes from 'Synapse' GO terms. Interestingly, this transcription factor was significantly upregulated in our RNA sequencing analysis (**Supplementary Table 1**). Nr4a1 is an orphan nuclear receptor that acts as a transcription factor, known to be induced by psychostimulants and capable of activity-dependently reshape synaptic functions [9-11]. As *Nr4a1* appeared to be a relevant target, we trained another cohort of mice in the same self-administration procedure in order to validate our sequencing and bioinformatics findings (**Supplementary Figure 1a**). Quantitative RT-PCR of VP tissue confirmed a significant increase of *Nr4a1* mRNA expression following cocaine intake (+162%; **Figure 1d**). Moreover, 42.9% of *Nr4a1* gene-targets identified by our transcriptional regulator analysis were significantly changed following cocaine intake (**Figure 1d**). We ran the same validation experiment in a cohort of female mice. We did not observe significant changes in Nr4a1 expression or any of its target suggesting *Nr4a1*-related changes were specific to males (**Supplementary Figure 1b, c**).

Our analyses highlighted GO terms and genes involved in dendritic spine remodeling. *Nr4a1* and some of its significantly upregulated gene targets such as *Plk2* (Polo-like kinase 2), *Dlgap2* (DLG Associated Protein 2) and *Rgs14* (Regulator Of G-Protein Signaling 14) are involved in

spine remodeling through the Ras/Raf GTPase signaling pathway [12-14]. To assess these potential structural plasticity changes, we exposed mice to cocaine for 10 days (20mg/kg, ip.) and 24h later we found that the activity of the small Ras GTPase Rap2 was significantly increased in the VP (**Figure 1e**) supporting potential dendritic spine remodeling [11, 12].

The VP sends outputs to various brain regions [1, 3, 6, 7]. We thus decided to investigate whether changes in Nr4a1 expression were restricted to specific VP projection subpopulations. We focused on 3 main VP projection populations known to be important for reward processing: the ventral tegmental area (VTA), the lateral habenula (LHb) and the mediodorsal thalamus (MDT) [1]. Following the injection of a retrograde Cre vector (AAV5-Cre-GFP) in each output structure, distinct groups of mice went through our self-administration procedure (**Supplementary Figure 2a**). Twenty-four hours later VP tissue was collected for *in situ* hybridization (**Figure 2a**). Colocalization quantification of *Cre*- and *Nr4a1*-positive cells revealed that a significantly lower proportion of VP neurons projecting to the VTA expressed *Nr4a1* after cocaine self-administration (-30%) while no changes were observed in neurons projecting to the LHb (**Figure 2b**). Interestingly, the VP neurons projecting to the MDT (VP→MDT) showed a significantly higher proportion of cells with *Nr4a1* expression (+40%; **Figure 2b**). To obtain a measure of mRNA expression levels in these different circuits, we also quantified *Nr4a1* puncta density in each projection. This analysis revealed that only the VP→MDT neurons had increased Nr4a1 puncta density following drug intake (+76%; **Figure 2c**). Together, our circuit analysis showed that only VP→MDT neurons, showed increases for both *Nr4a1* expression levels and the proportion of cells expressing *Nr4a1* after cocaine intake. We thus chose this specific projection population for further investigation.

As Nr4a1 is involved in structural plasticity and dendritic spine remodeling [11], we chose to pursue our studies with a 4-hour time-point that would allow us to assess dendritic spine dynamics [15]. RiboTag mice were injected with a retrograde Cre vector in the MDT and went

through the same cocaine self-administration protocol, except that VP tissue was collected 4 hours following the last session. Ribosome-associated mRNA from VP→MDT neurons was then immunoprecipitated and mRNA levels were measured with a multiplexed assay (**Figure 2d**). We selected 52 genes to both characterize the identity of VP→MDT neurons and measure changes in *Nr4a1* target genes and known structural plasticity-related molecules. Assessment of gene enrichment in the VP→MDT neurons from saline mice (**Figure 2e; Supplementary Table 3**) indicated that this cell-population expressed higher parvalbumin (*Pvalb*) and lower calbindin (*Calb1*) levels than the general VP. Information about neurotransmission in this cell subpopulation is scarce. The enrichment of *Gad1* (Glutamate Decarboxylase 1) and *Slc17a6* (*Vglut2*; Vesicular Glutamate Transporter 2) indicated that this projection contained both GABAergic and glutamatergic neurons [1, 7]. However, these cells expressed reduced proenkephalin (*Penk*) and substance P (*Tac1*) suggesting low peptidergic transmission. While *Chrna4* (Cholinergic Receptor Nicotinic α4 Subunit) was highly enriched in these cells, levels of *ChAT* (Choline Acetyltransferase) were comparable to bulk VP suggesting that these cells could be cholinoceptive rather than cholinergic [16]. VP→MDT cells also expressed higher levels of N-methyl-D-aspartate receptor subunits 1 and 2b (*Grin1* and *Grin2b*) as well as GABAergic receptor subunits α1 and β2 (*Gabra1* and *Gabrb2*). Additionally, VP→MDT neurons were highly enriched in Neurofilament Heavy Chain (*Nefh*; +332%). Future work will need to determine if this gene could be used to selectively target the VP→MDT subpopulation. Of note, these enrichment patterns were largely identical in mice taking cocaine, confirming that these genes were stable markers of this neuronal population (**Supplementary Figure 2c**).

Next, we compared changes in gene expression due to cocaine intake specifically in VP→MDT neurons (**Figure 2f; Supplementary Table 3**). We first confirmed increased *Nr4a1* levels after cocaine intake in this subpopulation at the 4h time-point (as well as in the whole VP: **Supplementary Figure 2c**). The *Nr4a1* upstream regulator *Mef2c* (Myocyte Enhancer Factor 2C) was also increased along with the *Nr4a1* downstream target *Plk2*. Plk2's downstream

targets *Sipa1l1* (Signal Induced Proliferation Associated 1 Like 1; or SPAR) showed high mRNA levels paralleled by low mRNA levels of *Rasgrf1* (Ras Protein Specific Guanine Nucleotide Releasing Factor 1) and high *Rap2a* levels, further supporting the role of this small GTPase signaling in our study and more largely in Nr4a1-mediated adaptations [11, 12]. Additionally, *Syn1* (Synapsin-1) levels were increased, supporting changes in synaptogenesis and neurotransmitter release. Surprisingly, although basal enrichment of *Penk* and *Tac1* in this cell-population was low, cocaine intake significantly increased levels of both these molecules. Peptidergic transmission originating from VP neurons is insufficiently characterized but our observations, supported by recent findings [2, 17], suggest that it could be involved in motivated behaviors.

Knowing that Nr4a1 is involved in structural plasticity and that its expression was increased in VP→MDT neurons following cocaine intake, we interrogated how artificially increasing *Nr4a1* levels (**Supplementary Figure 3a**) in this specific cell-population would impact cocaine intake and dendritic spine dynamics (**Figure 3a**). *Nr4a1* overexpression did not impact cocaine intake over 10 days (**Figure 3b**). Water self-administration was preserved as well (**Supplementary Figure 3b**). However, when tested for cocaine-seeking under extinction conditions, mice with Nr4a1 overexpression showed heightened active responding compared to controls (**Figure 3c**). Repeating these sessions showed no effect of *Nr4a1* overexpression on further extinction (**Figure 3d**). Finally, *Nr4a1* overexpression in VP→MDT neurons revealed sensitized response to a low dose of cocaine on drug-induced reinstatement (**Figure 3e**). Dendritic spines analysis 4h following the last cocaine exposure (**Figure 3f, g**) showed that although cocaine intake increased spine density in controls (+167.2% from eYFP saline), *Nr4a1* overexpression blocked this increase (-3.4% from eYFP saline) (**Figure 3h**). Together, this suggested that increased *Nr4a1* expression potentiated drug-seeking and relapse-like behavior while also blocking increased dendritic spine density. To further support these observations, we did the converse experiment (**Figure 3i**). Surprisingly, decreasing Nr4a1 expression (**Supplementary Figure 3c,**

d, e) using CRISPR-knockdown in VP→MDT neurons completely prevented the acquisition of cocaine self-administration (**Figure 3j**). Of note, water self-administration was preserved (**Supplementary Figure 3f**). Consequently, mice with *Nr4a1* knockdown showed no cocaine-seeking, extinction or sensitized drug-induced reinstatement (**Figure 3k, l, m**). Spine analysis (**Figure 3n, o**) confirmed increased spine density after cocaine intake in controls (+130.1% from LacZ saline). However, high spine density was also seen in mice with *Nr4a1* knockdown regardless of the drug condition (saline: +95.5%; cocaine: +74.7%; both from LacZ saline; **Figure 3p**) further supporting the role of Nr4a1 in dendritic spine dynamics.

Altogether, our study uncovers a role for *Nr4a1* in the VP, and more particularly VP→MDT neurons, in mediating addiction-like behaviors. In agreement with previous work, we show that *Nr4a1* expression negatively regulates dendritic spine density [11, 18] and that it bidirectionally modulates cocaine-mediated behaviors [10]. However, contrarily to previous findings in the nucleus accumbens [10], we showed that *Nr4a1* expression in VP→MDT neurons positively supports drug-seeking and relapse-like behaviors. Nr4a1 has a role in homeostatic mechanisms preventing cellular damage induced by neuronal overexcitation [9-11, 18]. It is likely that in VP→MDT neurons, homeostatic spine remodeling mechanisms induced by *Nr4a1* resulted in circuit adaptations facilitating pro-reward behaviors. This further demonstrates that similar protective mechanisms at the cellular levels can lead to opposite behavioral outcomes that can be either advantageous or deleterious depending on the brain region or cell-type.

Strikingly, while Nr4a1 has been involved in early and late cocaine abstinence [9, 10], our work showed that *Nr4a1* knockdown in VP impaired the development of cocaine intake. Nr4a1 is involved in spine remodeling mechanisms necessary for synaptic potentiation and memory formation [11, 19]. Prevention of structural plasticity with *Nr4a1* knockdown may have impaired the learning of the action-outcome association, for which VP and MDT are involved [20, 21]. Notably,

Nr4a1 knockdown did not impact water self-administration suggesting that the VP→MDT circuit may not be involved in learning action-outcome association for natural rewards. This circuit could thus be engaged in more complex, delayed rewards such as cocaine [22] consistent with the role of MDT in working memory and behavioral perseverance [23], and exemplified here with perseverative responding during drug-seeking after *Nr4a1* overexpression. While the exact cognitive mechanisms altered by cocaine intake remain to be clarified, our work demonstrated a significant role for the VP→MDT circuit in addiction-like behaviors through *Nr4a1*-mediated structural plasticity.

Acknowledgments

This work was funded by NIH grants R01MH106500, R01DA038613, R01DA047843 and Israel-US Binational Science Foundation 201725 (to MKL), K99DA050575 (to MEF), F31DA052967 (to EC), T32DK098107 and F32DA052966 (to CAC). SST and RJH were supported by the University of Maryland Scholars Program, an initiative of the University of Maryland: MPowering the State. The authors would like to thank the members of the UMSOM Institute for Genome Science (IGS) and Katherine Duarte for their technical help.

Author contributions

ME and MKL designed the experiments. ME, MEF, HQ, SST and RJH conducted behavioral experiments, MDT and VMR provided animal support. ME and HQ performed RAP2 assay. ME, EYC, RJH and VMR extracted RNA and/or performed qRT-PCR experiments. HN and ME performed *in situ* hybridization. MEF conducted cell-type specific RNA extraction. SST and ME performed *in situ* hybridization quantification. RC, EYC and CAC designed viral constructs. ME performed bioinformatic analyses. ME and MEF conducted neuronal morphology experiments. ME and MKL wrote the manuscript with contributions from all authors.

The authors declare that they have no conflict of interest.

References

1. Root, D.H., Melendez, R.I., Zaborszky, L. & Napier, T.C. The ventral pallidum: Subregion-specific functional anatomy and roles in motivated behaviors. *Prog Neurobiol* **130**, 29-70 (2015).

2. Heinsbroek, J.A.*, et al.* Opposing Regulation of Cocaine Seeking by Glutamate and GABA Neurons in the Ventral Pallidum. *Cell Rep* **30**, 2018-2027 e2013 (2020).

3. Tooley, J.*, et al.* Glutamatergic Ventral Pallidal Neurons Modulate Activity of the Habenula-Tegmental Circuitry and Constrain Reward Seeking. *Biol Psychiatry* **83**, 1012-1023 (2018).

4. Mahler, S.V.*, et al.* Designer receptors show role for ventral pallidum input to ventral tegmental area in cocaine seeking. *Nat Neurosci* **17**, 577-585 (2014).

5. Ottenheimer, D.J.*, et al.* A quantitative reward prediction error signal in the ventral pallidum. *Nat Neurosci* **23**, 1267-1276 (2020).

6. Faget, L.*, et al.* Opponent control of behavioral reinforcement by inhibitory and excitatory projections from the ventral pallidum. *Nat Commun* **9**, 849 (2018).

7. Levi, L.A.*, et al.* Projection-Specific Potentiation of Ventral Pallidal Glutamatergic Outputs after Abstinence from Cocaine. *J Neurosci* **40**, 1276-1285 (2020).

8. Knowland, D.*, et al.* Distinct Ventral Pallidal Neural Populations Mediate Separate Symptoms of Depression. *Cell* **170**, 284-297 e218 (2017).

9. Campos-Melo, D., Galleguillos, D., Sanchez, N., Gysling, K. & Andres, M.E. Nur transcription factors in stress and addiction. *Front Mol Neurosci* **6**, 44 (2013).

10. Carpenter, M.D.*, et al.* Nr4a1 suppresses cocaine-induced behavior via epigenetic regulation of homeostatic target genes. *Nat Commun* **11**, 504 (2020).

11. Chen, Y.*, et al.* Activity-induced Nr4a1 regulates spine density and distribution pattern of excitatory synapses in pyramidal neurons. *Neuron* **83**, 431-443 (2014).

12. Lee, K.J., Hoe, H.S. & Pak, D.T. Plk2 Raps up Ras to subdue synapses. *Small GTPases* **2**, 162-166 (2011).

13. Ranta, S.*, et al.* Positional cloning and characterisation of the human DLGAP2 gene and its exclusion in progressive epilepsy with mental retardation. *Eur J Hum Genet* **8**, 381-384 (2000).

14. Shu, F.J., Ramineni, S. & Hepler, J.R. RGS14 is a multifunctional scaffold that integrates G protein and Ras/Raf MAPkinase signalling pathways. *Cell Signal* **22**, 366-376 (2010).

15. Martin, J.A.*, et al.* A novel role for the actin-binding protein drebrin in regulating opiate addiction. *Nat Commun* **10**, 4140 (2019).

16. Young, W.S., 3rd, Alheid, G.F. & Heimer, L. The ventral pallidal projection to the mediodorsal thalamus: a study with fluorescent retrograde tracers and immunohistofluorescence. *J Neurosci* **4**, 1626-1638 (1984).

17. Macpherson, T., Mizoguchi, H., Yamanaka, A. & Hikida, T. Preproenkephalin-expressing ventral pallidal neurons control inhibitory avoidance learning. *Neurochem Int* **126**, 11-18 (2019).

18. Jeanneteau, F.*, et al.* The Stress-Induced Transcription Factor NR4A1 Adjusts Mitochondrial Function and Synapse Number in Prefrontal Cortex. *J Neurosci* **38**, 1335-1350 (2018).

19. Hawk, J.D.*, et al.* NR4A nuclear receptors support memory enhancement by histone deacetylase inhibitors. *J Clin Invest* **122**, 3593-3602 (2012).

20. Corbit, L.H., Muir, J.L. & Balleine, B.W. Lesions of mediodorsal thalamus and anterior thalamic nuclei produce dissociable effects on instrumental conditioning in rats. *Eur J Neurosci* **18**, 1286-1294 (2003).

21. Leung, B.K. & Balleine, B.W. Ventral pallidal projections to mediodorsal thalamus and ventral tegmental area play distinct roles in outcome-specific Pavlovian-instrumental transfer. *J Neurosci* **35**, 4953-4964 (2015).

22. Canchy, L., Girardeau, P., Durand, A., Vouillac-Mendoza, C. & Ahmed, S.H. Pharmacokinetics trumps pharmacodynamics during cocaine choice: a reconciliation with the dopamine hypothesis of addiction. *Neuropsychopharmacology* **46**, 288-296 (2021).

23. Parnaudeau, S.*, et al.* Inhibition of mediodorsal thalamus disrupts thalamofrontal connectivity and cognition. *Neuron* **77**, 1151-1162 (2013).

Figure legends

Figure 1

Cocaine intake alters structural plasticity-related molecules in the ventral pallidum. **a**: Number of infusions acquired during the 10 days of self-administration. Mice from the cocaine group obtained significantly more infusions than mice from the saline group ($p < 0.01$ from day 3 onward). n= 4 per group; **b**: Ventral pallidum tissue was collected 24 hours following self-administration and used for RNA sequencing. Heat map for the 363 genes showing significant False Discovery Rate (FDR; $p < 0.05$). From these 363, genes 46.8% were downregulated and 53.2% were upregulated; **c**: Gene Ontology analysis (GO) revealed a high number of significant GO terms related to neuronal morphology and structural plasticity. Of note, neuronal morphology-related GO terms represented 40.6% of the “Cellular Component” GO terms. These morphology-related GO terms included 200 unique genes, which represented 55% of all the significantly differentially expressed genes; **d**: Left bar graph: Transcriptional regulator analysis of significant “Cellular component” -related genes, identified Nr4a1 (Nurr 77) as a potential common regulator. Subsequent qRT-PCR analysis confirmed RNAseq data and showed a significant increase of Nr4a1 expression in the VP 24 hours following 10 days of cocaine self-administration ($p < 0.01$). Right heat maps: qRT-PCR analyses further confirmed significant changes in multiple Nr4a1 target genes initially identified with RNAseq and bioinformatics analyses ($p < 0.05$ at least). For RNAseq n= 4 per group and for qRT-PCR, n= 7 per group; **e** Rap2 activity assay was conducted 24 hours following 10 days of cocaine (20/mg/kg, i.p. in saline) or saline exposure. Rap2 activity was increased in the VP of mice exposed to cocaine ($p<0.05$). n= 7 per group. Detailed statistics are available in Supplementary Material 1. See also Supplementary Figure 1 for additional information.

Figure 2

Cocaine intake alters Nr4a1 and morphology-related genes specifically in VP neurons projecting to MDT. **a**: Schematic of the experimental design: 3 different groups of mice received an infusion of retrograde (AAV5) Cre-GFP vector in either the ventral tegmental area (VTA), the lateral habenula (LHb) or the mediodorsal thalamus (MDT). Animals were then subjected to either cocaine (0.5 mg/kg/inf.) or saline self-administration for 10 days. Twenty-four hours later, brain sections containing the ventral pallidum (VP) were collected for fluorescent *in situ* hybridization; **b**: Proportion of Cre-positive cells expressing Nr4a1 among all the Cre-positive cells in each group. A significantly lower proportion of VP cells projecting to the VTA expressed Nr4a1 in mice taking cocaine compared to saline controls ($p< 0.01$). Oppositely, a significantly higher proportion of VP cells projecting to the MDT expressed Nr4a1 in mice taking cocaine compared to saline controls ($p< 0.001$). n= 5 in each group; **c**: Nr4a1 puncta density (puncta per Cre-positive cell) was assessed for each group. Only VP cells projecting to the MDT showed a significantly higher Nr4a1 expression level following cocaine intake compared to saline control ($p< 0.05$). n= 5 per group; density was measured from 120 Cre-positive cells per animal. Right panel: representative image from VP cells projecting to the MDT from each group, scale bar= 20 μm; **d**: Schematic of the experimental design: RiboTag mice were injected with retrograde (AAV5) Cre-GFP vectors. Animals were subjected to 10 days of cocaine (0.5 mg/kg/inf.) or saline self-administration and VP tissue was collected 4 hours following the last session. Tagged polyribosomes from VP to MDT neurons were then immunoprecipitated, mRNA was isolated and gene expression was analyzed using a multiplexed gene expression assay. n= 4-5 mice per sample, 6 samples per condition; **e**: Heat map representing gene enrichment in VP to MDT neurons in saline control mice ($p\leq 0.05$ at least); **f**: Heat map showing differences in gene expression, specifically in VP to MDT neurons, in mice taking cocaine compared to mice taking

saline ($p \leq 0.05$ at least). Detailed statistics are available Supplementary Material 1 and in Supplementary Table 3. See also Supplementary Figure 2 for additional information.

Figure 3

Bidirectional manipulation of Nr4a1 in VP to MDT neurons oppositely regulates cocaine-related behaviors and dendritic spine density. **a**: Schematic of the experimental design: mice received an infusion of retrograde (AAV5) Cre-GFP vector in the MDT and an infusion of DIO-Nr4a1-eYFP (or DIO-eYFP) + DIO-mCherry in the VP prior to cocaine (0.5 mg/kg/inf.) or saline self-administration. The day following the last self-administration session, mice were subjected to seeking test (under extinction condition) as well as 5 additional extinction sessions. The next day, mice were tested for drug-induced reinstatement. Four hours following this last test, tissue was collected for spine density evaluation. n= 6 eYFP-saline, 10 eYFP-cocaine, 5 Nr4a1-saline, 8 Nr4a1-cocaine; **b**: Mice with Nr4a1 overexpression in VP to MDT neurons acquired cocaine self-administration at levels comparable to eYFP controls. Both groups show significantly higher intake compared to their respective controls ($p < 0.05$ at least); **c**: Both groups showed significant seeking behavior compared to their respective saline controls. However, mice with Nr4a1 overexpression showed higher levels of active responses compared to eYFP overexpression mice ($p < 0.05$ at least). Insert represents cumulative active response in cocaine mice during the 1 hour seeking test (5 min bins); **d**: Active responses during extinction test. Both groups show similar rate of extinction ($p < 0.05$ from respective saline controls); **e**: Animals previously taking cocaine were exposed to non-contingent cocaine for drug-induced reinstatement (7.5 mg/kg, i.p.; saline controls received saline, i.p.). While eYFP-cocaine mice showed a trend in increased active responses, Nr4a1-cocaine mice made significantly more active responses compared to their respective control ($p < 0.05$); **f**: Left panel: Representative image of MDT injection site for retrograde (AAV5) Cre-GFP viral vector. Right panel: Representative image of Nr4a1 positive

cells in mice with Nr4a1 overexpression and sparse DIO-mCherry labelling in the VP. Closed arrowhead: Nr4a1+mCherry positive cell, open arrowhead: Nr4a1 positive cell. Scale bars= 25 μm; **g**: Representative image of dendritic spines from sparsely labelled VP to MDT neurons from each group. Scale bar= 5 μm; **h**: Spine density was significantly increased in control mice taking cocaine while Nr4a1 overexpression blocked this increase ($p< 0.01$); **i**: Schematic of the experimental design: mice received an infusion of retrograde (AAV5) Cre-GFP vector in the MDT and an infusion of DIO-SaCas9 + Nr4a1-sagRNAx3-eGFP (or LacZ-sagRNAx3-eGFP) + DIO-mCherry in the VP prior to cocaine (0.5 mg/kg/inf.) or saline self-administration. The day following the last self-administration session, mice were subjected to seeking test (under extinction condition) as well as 5 additional extinction sessions. The next day, mice were tested for drug-induced reinstatement. Four hours following this last test, tissue was collected for spine density evaluation. n= 7 LacZ-saline, 7 LacZ-cocaine, 8 Nr4a1-gRNA-saline, 6 Nr4a1-gRNA-cocaine; **j**: Mice with Nr4a1 knockdown in VP to MDT neurons did not acquire cocaine self-administration and showed intake levels comparable to saline controls (*$p< 0.05$ from respective saline, #$p< 0.05$ from LacZ-cocaine mice); **k**: LacZ-cocaine showed significant seeking behavior compared to their respective saline controls as well as compared to Nr4a1-gRNA-cocaine mice ($p< 0.01$ and $p< 0.001$ respectively). Insert represents cumulative active response in cocaine mice during the 1 hour seeking test (5 min bins); **l**: Active responses during extinction test; **m**: Animals previously taking cocaine were exposed to non-contingent cocaine for drug-induced reinstatement (7.5 mg/kg, i.p.; saline controls received saline, i.p.). None of the groups showed enhanced responding following exposure to a low dose of cocaine; **n**: Left panel: Representative image of MDT injection site for retrograde (AAV5) Cre-GFP viral vector. Right panel: Representative image of cells with Nr4a1 knockdown (DIO-SaCas9 + Nr4a1-gRNA) and sparse DIO-mCherry labelling in the VP. Closed arrowhead: SaCas9+Nr4a1-gRNA+mCherry positive cell, open arrowhead: SaCas9+Nr4a1-gRNA positive cell. Scale bars= 25 μm; **o**: Representative image of dendritic spines from sparsely labelled VP to MDT neurons from each group. Scale

bar= 5 μm; **p**: Spine density was significantly increased in control mice taking cocaine. Both groups of mice with Nr4a1 knockdown showed elevated spine density levels that did not differ from control mice taking cocaine ($p < 0.05$, ns: not significant). Detailed statistics are available in Supplementary Material 1. See also Supplementary Figure 3 for additional information. Hipp: hippocampus, D3V: dorsal 3rd ventricle, MHb: medial habenula, LHb: lateral habenula, sm: stria medularis, PV: paraventricular thalamic nucleus, MDT: mediodorsal thalamus, PC: paracentral thalamic nucleus.

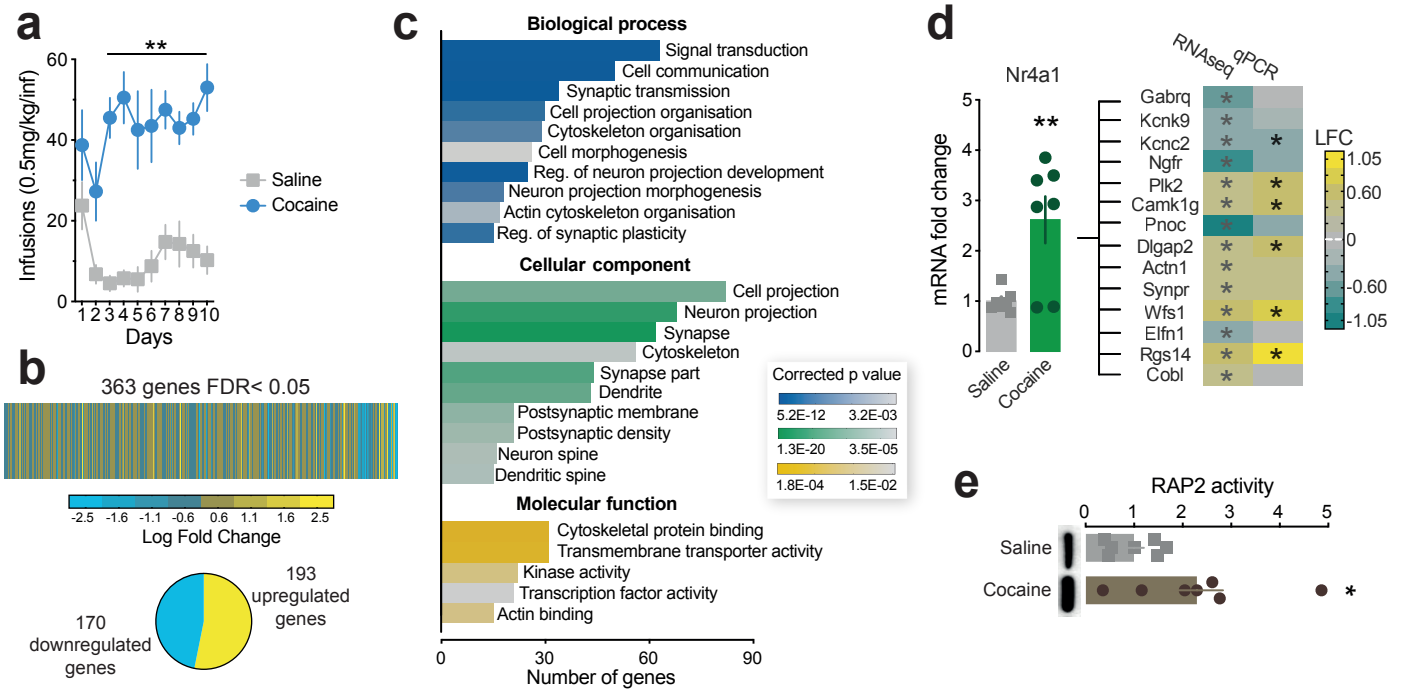
a
**
Infusions (0.5mg/kg/inf)
60
40
20
0
1 2 3 4 5 6 7 8 9 10
Days
Saline
Cocaine
b
363 genes FDR< 0.05
-2.5 -1.6 -1.1 -0.6 0.6 1.1 1.6 2.5
Log Fold Change
193
upregulated
genes
170
downregulated
genes
c
Biological process
Signal transduction
Cell communication
Synaptic transmission
Cell projection organisation
Cytoskeleton organisation
Cell morphogenesis
Reg. of neuron projection development
Neuron projection morphogenesis
Actin cytoskeleton organisation
Reg. of synaptic plasticity
Cellular component
Cell projection
Neuron projection
Synapse
Cytoskeleton
Synapse part
Dendrite
Postsynaptic membrane
Postsynaptic density
Neuron spine
Dendritic spine
Molecular function
Cytoskeletal protein binding
Transmembrane transporter activity
Kinase activity
Transcription factor activity
Actin binding
Corrected p value
5.2E-12 3.2E-03
1.3E-20 3.5E-05
1.8E-04 1.5E-02
0
30
60
90
Number of genes
d
Nr4a1
mRNA fold change
5
4
3
2
1
0
**
Saline
Cocaine
RNAseq
qPCR
Gabrq
Kcnk9
Kccn2
Ngfr
Plk2
Camk1g
Pnoc
Dlgap2
Actn1
Synpr
Wfs1
Elfn1
Rgs14
Cobl
LFC
1.05
0.60
0
-0.60
-1.05
e
RAP2 activity
0
1
2
3
4
5
Saline
Cocaine
*

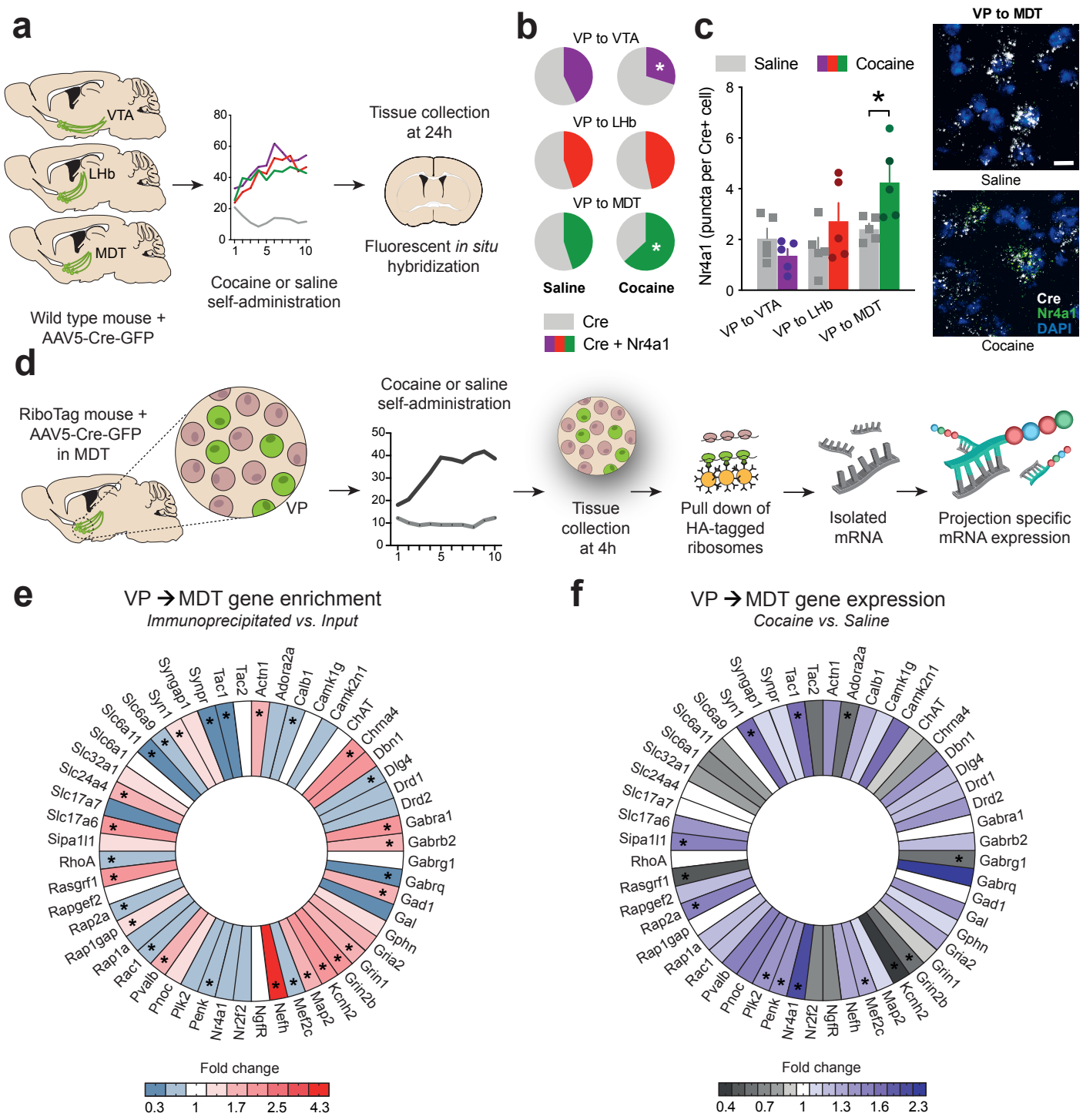
a
VTA
LHb
MDT
Wild type mouse +
AAV5-Cre-GFP
Cocaine or saline
self-administration
Tissue collection
at 24h
Fluorescent *in situ*
hybridization
b
VP to VTA
VP to LHb
VP to MDT
Saline
Cocaine
Cre
Cre + Nr4a1
c
Saline
Cocaine
Nr4a1 (puncta per Cre+ cell)
VP to VTA
VP to LHb
VP to MDT
VP to MDT
Saline
Cre
Nr4a1
DAPI
Cocaine
d
RiboTag mouse +
AAV5-Cre-GFP
in MDT
VP
Cocaine or saline
self-administration
Tissue
collection
at 4h
Pull down of
HA-tagged
ribosomes
Isolated
mRNA
Projection specific
mRNA expression
e
VP → MDT gene enrichment
Immunoprecipitated vs. Input
Syngap1
Synpr
Tac1
Tac2
Actn1
Adora2a
Calb1
Camk1g
Camk2n1
ChAT
Chrna4
Dbn1
Dlg4
Drd1
Drd2
Gabra1
Gabrb2
Gabrg1
Gabrq
Gad1
Gal
Gphn
Gria2
Grin1
Grin2b
Kcnn2
Map2
Mef2c
Nefh
NgfR
Nr2f2
Nr4a1
Penk
Plk2
Pnoc
Pvalb
Rac1
Rap1a
Rap1gap
Rap2a
Rapgef2
Rasgrf1
RhoA
Sipa1l1
Slc17a6
Slc17a7
Slc24a4
Slc32a1
Slc6a1
Slc6a11
Slc6a9
Syn1
Fold change
0.3
1
1.7
2.5
4.3
f
VP → MDT gene expression
Cocaine vs. Saline
Fold change
0.4
0.7
1
1.3
1.6
2.3

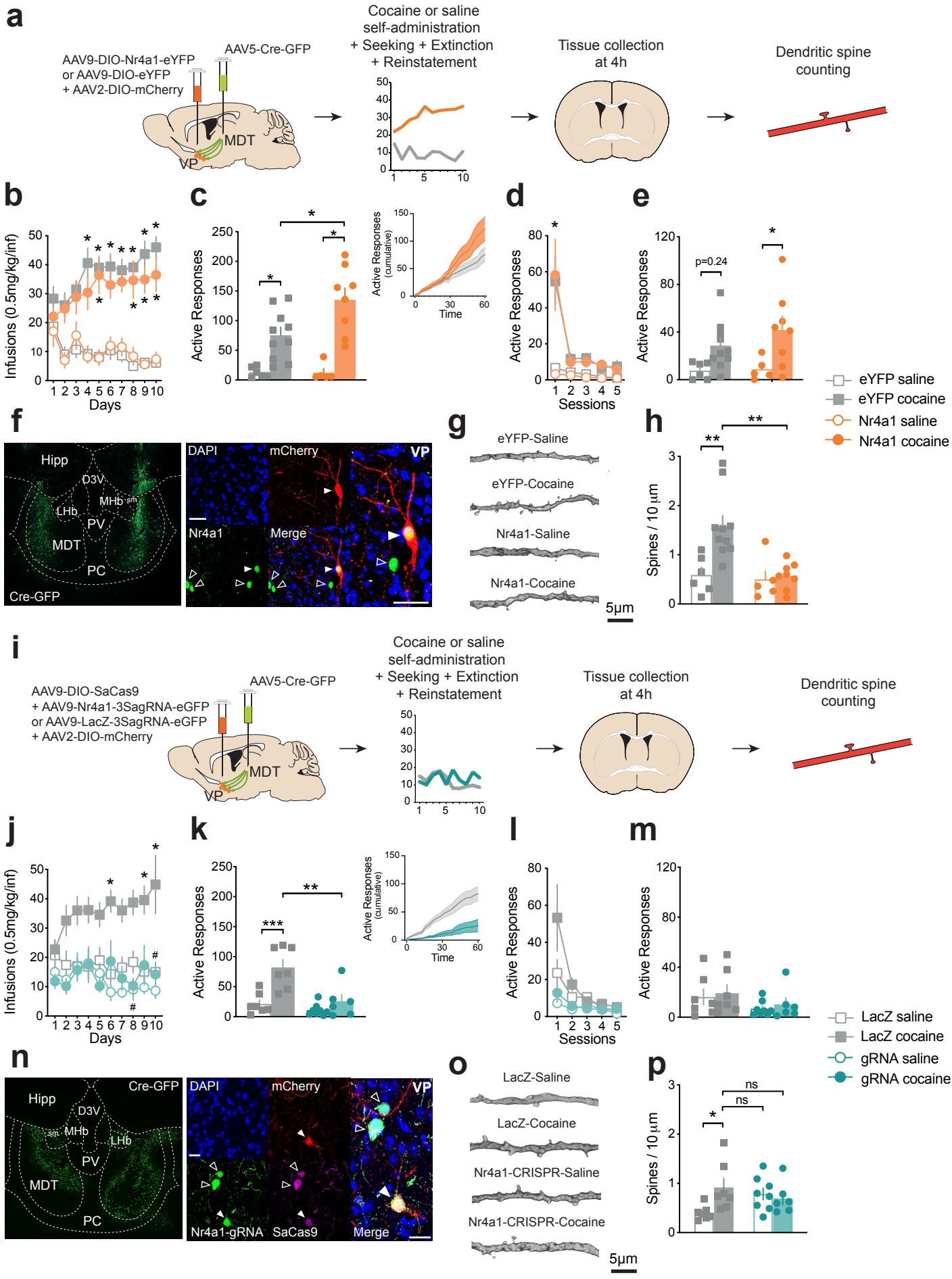
a
AAV9-DIO-Nr4a1-eYFP
or AAV9-DIO-eYFP
+ AAV2-DIO-mCherry
AAV5-Cre-GFP
MDT
VP
Cocaine or saline
self-administration
+ Seeking + Extinction
+ Reinstatement
Tissue collection
at 4h
Dendritic spine
counting
b
Infusions (0.5mg/kg/inf)
Days
c
Active Responses
Active Responses
(cumulative)
Time
d
Active Responses
Sessions
e
Active Responses
p=0.24
eYFP saline
eYFP cocaine
Nr4a1 saline
Nr4a1 cocaine
f
Hipp
D3V
LHb
MHb
sm
PV
MDT
PC
Cre-GFP
DAPI
mCherry
VP
Nr4a1
Merge
g
eYFP-Saline
eYFP-Cocaine
Nr4a1-Saline
Nr4a1-Cocaine
5µm
h
Spines / 10 µm
i
AAV9-DIO-SaCas9
+ AAV9-Nr4a1-3SagRNA-eGFP
or AAV9-LacZ-3SagRNA-eGFP
+ AAV2-DIO-mCherry
AAV5-Cre-GFP
MDT
VP
Cocaine or saline
self-administration
+ Seeking + Extinction
+ Reinstatement
Tissue collection
at 4h
Dendritic spine
counting
j
Infusions (0.5mg/kg/inf)
Days
k
Active Responses
Active Responses
(cumulative)
Time
l
Active Responses
Sessions
m
Active Responses
LacZ saline
LacZ cocaine
gRNA saline
gRNA cocaine
n
Hipp
Cre-GFP
D3V
sm
MHb
LHb
PV
MDT
PC
DAPI
mCherry
VP
Nr4a1-gRNA
SaCas9
Merge
o
LacZ-Saline
LacZ-Cocaine
Nr4a1-CRISPR-Saline
Nr4a1-CRISPR-Cocaine
5µm
p
Spines / 10 µm
ns

Transcriptome profiling of the ventral pallidum reveals a role for pallido-thalamic neurons in cocaine reward

Michel Engeln[1,2,#], Megan E. Fox[1,3], Ramesh Chandra[1], Eric Y. Choi[1], Hyungwoo Nam[1], Houman Qadir[1], Shavin S. Thomas[1], Victoria M. Rhodes[1], Makeda D. Turner[1], Rae J. Herman[1], Cali A. Calarco[1], Mary Kay Lobo[1#].

1. Department of Anatomy and Neurobiology, University of Maryland School of Medicine, Baltimore, MD, USA.
2. University of Bordeaux, CNRS, IMN, UMR 5293, F-33000 Bordeaux, France.
3. Department of Anesthesiology & Perioperative Medicine, Penn State College of Medicine, Hershey, PA, USA.

Results

Mice developed self-administration and showed significantly higher numbers of cocaine infusions compared to saline starting at day 3: 2-way RM ANOVA: Day x Drug: $F_{(9, 54)}$= 2.7; p= 0.011; Sidak posthoc: p< 0.01 at least (**Figure 1a**). Ventral pallidum tissue was collected 24 hours after the last drug intake session and processed for RNA sequencing. Out of the 32,787 genes identified with RNA sequencing, 363 genes (1.11%) were differentially expressed in mice taking cocaine compared to saline: FDR< 0.05 (please see **Suppl Table 1** for detailed RNA sequencing results). From this subset of genes, 170 (46.8%) were downregulated and 193 (53.2%) were upregulated (**Figure 1b**). Gene ontology (GO) has been conducted using the 363 significantly differentially expressed (SDE) genes. At the “Biological process” level, the GO analysis did not retrieve some genes based on their name (e.g., predicted genes). The analysis was thus conducted on 311 SDE genes. Several GO terms were associated with neuronal

morphology and neuronal communication. Among them we found, 'Signal transduction' (GO:0007165; 63 genes; 20.3% frequency in set; Corrected p< 4.7844E-6), 'Cell communication' (GO:0007154; 50 genes; 16.1% frequency in set; Corrected p< 2.3360E-11), 'Synaptic transmission' (GO:0007268; 34 genes; 10.9% frequency in set; Corrected p< 5.1779E-12), 'Cell projection organization' (GO:0030030; 30 genes; 9.6% frequency in set; Corrected p< 5.0450E-4), 'Cytoskeleton organization' (GO:0007010; 29 genes; 9.3% frequency in set; Corrected p< 1.0077E-3), 'Cell morphogenesis' (GO:0000902; 26 genes; 8.4% frequency in set; Corrected p< 3.2127E-3), 'Regulation of neuron projection development' (GO:0010975; 25 genes; 8% frequency in set; Corrected p< 4.7844E-6), 'Neuron projection morphogenesis' (GO:0048812; 18 genes; 5.8% frequency in set; Corrected p< 8.1937E-4), 'Actin cytoskeleton organization' (GO:0030036; 17 genes; 5.5% frequency in set; Corrected p< 2.5829E-3), 'Regulation of synaptic plasticity' (GO:0048167; 15 genes; 4.8% frequency in set; Corrected p< 5.2424E-4) (**Figure 1c**).

At the "Cellular component" level, the GO analysis did not retrieve some genes based on their name. The analysis was thus conducted on 319 SDE genes. Interestingly, neuronal morphology-related GO terms represented 40.6% of the "Cellular Component" GO terms. There were 200 unique genes in the morphology-related GO terms, which represents 55% of all the SDE genes and 63% of the SDE genes used for the GO analysis at the Cellular component level. Among the significant neuronal morphology-related GO terms, we found: 'Cell projection' (GO:0042995; 82 genes; 25.7% frequency in set; Corrected p< 1.9094E-14), 'Neuron projection' (GO:0043005; 68 genes; 21.3% frequency in set; Corrected p< 1.4402E-19), 'Synapse' (GO:0045202; 62 genes; 19.4% frequency in set; Corrected p< 1.2420E-20), 'Cytoskeleton' (GO:0005856; 56 genes; 17.6% frequency in set; Corrected p< 3.4743E-5), 'Synapse part' (GO:0044456; 44 genes; 13.8% frequency in set; Corrected p< 6.9172E-16), 'Dendrite' (GO:0030425; 43 genes; 13.5% frequency in set; Corrected p< 1.5502E-15), 'Postsynaptic membrane' (GO:0045211; 21 genes; 6.6% frequency in set; Corrected p< 1.3784E-9), 'Postsynaptic density' (GO:0014069; 21 genes;

6.6% frequency in set; Corrected p< 8.2744E-8), 'Neuron spine' (GO:0044309; 16 genes; 5% frequency in set; Corrected p< 1.0984E-7), 'Dendritic spine' (GO:0043197; 15 genes; 4.7% frequency in set; Corrected p< 4.6394E-7) (**Figure 1c**).

Finally, at the "Molecular function" level, the GO analysis did not retrieve some genes (based on their name). The analysis was thus conducted on 310 SDE genes. Among the relevant significant GO terms, we found: 'Cytoskeletal protein binding' (GO:0008092; 31 genes; 10% frequency in set; Corrected p< 1.8242E-4), 'Transmembrane transporter activity' (GO:0022857; 31 genes; 10% frequency in set; Corrected p< 2.8033E-4), 'Kinase activity' (GO:0016301; 22 genes; 7.1% frequency in set; Corrected p< 8.3849E-3), 'Transcription factor activity' (GO:0003700; 21 genes; 6.8% frequency in set; Corrected p< 1.5338E-2), 'Actin binding' (GO:0003779; 15 genes; 4.8% frequency in set; Corrected p< 8.9181E-3) (**Figure 1c**). Based on these results, transcriptional regulator analysis on genes from significant GO terms at the "Cellular component" level was run using iRegulon. Direct motif similarity was found between the transcription factor Nr4a1 and: 13 genes (19.1%) from the GO term 'Neuron projection' (Normalized Enrichment Score (NES): 3.165), 10 genes (16.1%) from the GO term 'Synapse' (NES: 3.455) and 4 genes (19%) from the GO term 'Postsynaptic membrane' (NES: 3.172) (**Figure 1d**).

Since bioinformatics analyses pointed toward changes in Nr4a1 and its target genes in neuronal morphology adaptations, we evaluated these changes in a new cohort of mice using qRT-PCR (**Figure 1d;** please see **Suppl Table 2** for primer sequences).

	RNA sequencing		qRT-PCR validation		
Gene name	LFC	FDR	LFC	t-test	p-value
Nr4a1	0.49	4,35E-05***	1.39	t_{12}= 3.425	p= 0.005**
Gabrq	-0.60	0.023*	-0.01	t_{12}= 0.063	p= 0.950
Kcnk9	-0.50	0.042*	-0.13	t_{12}= 0.532	p= 0.604
Kcnc2	-0.43	0.017*	-0.43	t_{12}= 2.919	p= 0.012*
Ngfr	-0.77	4,97E-08***	-0.49	t_{12}= 1.386	p= 0.191
Plk2	0.43	0.026*	0.64	t_{12}= 2.359	p= 0.036*
Camk1g	0.40	0.042*	0.60	t_{12}= 2.409	p= 0.033*
Pnoc	-1.17	4,40E-07***	-0.45	t_{12}= 1.867	p= 0.086
Dlgap2	0.47	3,55E-05***	0.69	t_{12}= 2.839	p= 0.014*
Actn1	0.44	0.014*	0.48	t_{12}= 1.057	p= 0.311
Synpr	0.44	0.016*	0.44	t_{12}= 1.066	p= 0.307
Wfs1	0.50	0.024*	0.8	t_{12}= 3.316	p= 0.006**
Elfn1	-0.45	0.009**	0.08	t_{12}= 0.361	p= 0.724
Rgs14	0.51	0.002**	1.1	t_{12}= 3.274	p= 0.006**
Cobl	0.40	0.032*	0.03	t_{12}= 0.143	p= 0.888

LFC: Log Fold Change; FDR: False Discovery Rate.

Since our bioinformatics and validation analyses highlighted genes that are involved in spine remodeling through the Ras/Raf GTPase signaling pathway, we further investigated changes in RAP activity in the VP following cocaine exposure. The RAP2 activity assay revealed that 10 days of cocaine exposure (20mg/kg, ip) induced a significant increase in RAP2 activity in the ventral pallidum (VP): t_{12} = 2.272; p= 0.0423 (**Figure 1e**).

In order to investigate whether changes in Nr4a1 expression occurred in all VP neurons or were restricted to specific neuronal subpopulations, we focused on 3 main VP projection populations important for reward processing: the ventral tegmental area (VTA), the lateral habenula (LHb) and the mediodorsal thalamus (MDT) (**Figure 2a**). When looking at the VP neurons projecting to the ventral tegmental area (VTA), the proportion of cells expressing Nr4a1 (Cre + Nr4a1) was significantly decreased in mice taking cocaine (29.8%) compared to saline controls (42.9%): Chi^2= 6.895, p= 0.0086. This proportion was not changed in VP neurons projecting to the lateral habenula (LHb) between animals taking cocaine (46.7%) or saline (44.8%): Chi^2= 0.162, p= 0.69. Interestingly, the proportion of VP neurons projecting to the mediodorsal thalamus (MDT) expressing Nr4a1 was increased in mice taking cocaine (63.2%) compared to saline controls (45%): Chi^2= 13.091, p= 0.0003 (**Figure 2b**). Evaluating the number of Nr4a1 puncta per cell in

these 3 projection neurons revealed that only the VP neurons projecting to the MDT showed increased (+76%) Nr4a1 expression levels following cocaine self-administration: 2-way ANOVA: Projection x Drug: $F_{(2, 24)}$= 3.54; p= 0.045; Sidak posthoc: p< 0.05 (**Figure 2c**). In a cohort of RiboTag mice subjected to cocaine self-administration, VP tissue was collected 4 hours following the last session. VP→MDT neurons were immunoprecipitated and mRNA levels were measured with a multiplexed assay (**Figure 2d**). We selected 52 genes to both characterize the identity of VP→MDT neurons and measure changes in Nr4a1 target genes and known structural plasticity-related molecules please see **Suppl Table 2** for primer sequences). Enrichment for Actn1, Chrna4, Dlg4, Gabra1, Gabrb2, Gad1, Grin1, Grin2b, Kcnh2, Map2, Nefh, Pvalb, Rasgfr1, Slc17a6, Slc24a4 and Syn1 was significantly increased in VP→MDT neurons (Please see **Suppl Table 3** for detailed statistics). Oppositely, enrichment for Calb1, Dlg4, Gabrq, Mef2c, Penk, Rac1, Rap1gap, Rap2a, RhoA, Slc6a11, Slc6a9, Synpr and Tac1 was significantly decreased in VP→MDT neurons (Please see **Suppl Table 3** for detailed statistics) (**Figure 2e**). We then compared changes in gene expression due to cocaine intake specifically in VP→MDT neurons (**Figure 2f**). Enrichment in Mef2c, Nr4a1, Penk, Plk2, Rap2a, Sipa1l1, Syn1 and Tac1 was significantly increased (Please see **Suppl Table 3** for detailed statistics). However, enrichment in Adora2a, Gabrg1, Grin2b, Kcnh2 and Rasgrf1 was significantly decreased in this neuronal subpopulation (Please see **Suppl Table 3** for detailed statistics).

To interrogate the role of Nr4a1 in cocaine-related behaviors we overexpressed Nr4a1 in VP→MDT neurons (**Figure 3a, f**). Cocaine and saline self-administration were compared in mice with Nr4a1 or eYFP overexpression in VP→MDT neurons. A 3-way ANOVA showed a significant Day x Drug interaction: Day x Drug: $F_{(9, 41)}$= 8.803; p< 0.0001 but no Day x Virus interaction: Day x Virus: $F_{(9, 171)}$= 0.468; p= 0.894, suggesting that both mice with eYFP and Nr4a1 overexpression were taking more doses of cocaine compared to their saline counterparts, although there were no differences in acquisition rate between the two groups taking cocaine.

Tukey's multiple comparison showed that eYFP mice were taking more doses compared to their respective control group from day 4 onward ($p< 0.05$ at least). This difference was observed in mice with Nr4a1 overexpression at day 5 and day 8 onward ($p< 0.05$) (**Figure 3b**). Mice were then tested for cocaine seeking behavior. Both mice with Nr4a1 or eYFP overexpression in VP→MDT neurons showed significant seeking behavior compared to their respective saline controls. However, mice with Nr4a1 overexpression previously taking cocaine showed higher levels of active responses compared to mice with eYFP overexpression previously taking cocaine: 2-way ANOVA: Drug: $F_{(1, 25)}= 37.23$; $p< 0.0001$; Drug x Virus: $F_{(1, 25)}= 3.93$; $p= 0.058$; Tukey posthoc: $p< 0.05$ at least (**Figure 3c**). Following seeking test, mice were evaluated for extinction in similar test conditions. A 3-way ANOVA showed a significant Session x Drug interaction: Session x Drug: $F_{(4, 11)}= 9.005$; $p< 0.01$ but no Session x Virus interaction: Session x Virus: $F_{(4, 76)}= 0.024$; $p= 0.998$ suggesting again that both mice with eYFP and Nr4a1 overexpression previously taking cocaine were making more active responses compared to their saline counterparts, although there were no differences in extinction rate between the two groups previously taking cocaine. Tukey's multiple comparison showed that both mice with eYFP and Nr4a1 overexpression, previously taking cocaine, made more active responses than their respective saline controls on Session 1: $p< 0.01$ (**Figure 3d**). Finally on the next day, mice were tested for drug induced reinstatement. A 2-way ANOVA highlighted a Drug effect suggesting that the low dose of cocaine increased the number of active responses in mice previously taking cocaine: 2-way ANOVA: Drug: $F_{(1, 25)}= 11.06$; $p= 0.002$. A Tukey multiple comparison revealed however that only mice previously exposed to cocaine with Nr4a1 overexpression showed significantly increased responding compared to their respective controls ($p= 0.050$). This was not observed for similar conditions in mice with eYFP overexpression ($p= 0.245$) (**Figure 3e**). Four hours following the drug-induced reinstatement test, mice were perfused and dendritic spine density was assessed in VP→MDT neurons (**Figure 3g**). A 2-way ANOVA showed a significant Drug x Virus interaction: Drug x Virus: $F_{(1, 25)}= 5.841$; $p= 0.023$.

Tukey posthoc test revealed that spine density was higher in mice with eYFP overexpression previously taking cocaine compared to their respective saline controls ($p< 0.01$) but also compared to mice with Nr4a1 overexpression previously taking cocaine ($p< 0.01$) (**Figure 3h**). In another set of experiments, cocaine and saline self-administration was compared in mice with Nr4a1 CRISPR knockdown or LacZ control in VP→MDT neurons (**Figure 3i, n**). A 3-way ANOVA showed a significant Day x Drug interaction: Day x Drug: $F_{(9, 64)}= 3.392$; $p= 0.001$ suggesting that mice developed cocaine self-administration over the 10 days. However a Drug x Virus interaction: Drug x Virus: $F_{(1, 16)}= 8.054$; $p= 0.011$ further suggested that viral manipulation had an effect of the acquisition of FR1. Tukey's multiple comparison revealed that LacZ control mice developed cocaine self-administration and were taking more doses compared to their respective saline group for days 6, 9 and 10 ($p\leq 0.05$ at least). Interestingly, such difference in mice with Nr4a1 CRISPR knockdown was never observed across the 10 days ($p>0.999$). Moreover, mice with Nr4a1 CRISPR knockdown took significantly less cocaine than their LacZ counterparts for days 8 and 10 ($p= 0.009$ and 0.002 respectively) (**Figure 3j**). Next, the mice were tested for cocaine seeking behavior. A 2-way ANOVA revealed that both previous drug exposure and viral manipulation had an effect on seeking behavior: Drug x Virus: $F_{(1, 24)}= 5.770$; $p= 0.024$. Tukey posthoc showed that mice with LacZ gRNA in VP→MDT neurons previously taking cocaine had significantly higher active responses compared to their respective saline controls ($p< 0.0007$), but also higher responses compared to mice with Nr4a1 CRISPR knockdown previously taking cocaine ($p< 0.002$) (**Figure 3k**). Following seeking test, mice were evaluated for extinction in similar test conditions. A 3-way ANOVA showed that extinction rate was different depending on the viral manipulation: Session x Virus: $F_{(4, 12)}= 6.626$; $p= 0.005$. Tukey posthoc showed that mice with LacZ gRNA in VP→MDT neurons previously taking cocaine had significantly higher active responses compared to their respective saline controls ($p= 0.002$) and compared to mice with Nr4a1 CRISPR knockdown previously taking cocaine ($p= 0.004$) for session 1 (**Figure 3l**). Finally, the following day mice were tested for drug-induced

reinstatement. Response levels were low in every group and the 2-way ANOVA reported no effect of our low doses of cocaine on active responses: 2-way ANOVA: Drug: $F_{(1, 24)}$= 0.375; p= 0.545 (**Figure 3m**). Mice were perfused four hours following the drug-induced reinstatement test and dendritic spine density was assessed in VP→MDT neurons (**Figure 3o**). A 2-way ANOVA showed a significant Drug x Virus interaction: Drug x Virus: $F_{(1, 24)}$= 5.257; p= 0.030. Tukey posthoc test revealed that spine density was higher in mice with LacZ control previously taking cocaine compared to their respective saline controls (p< 0.05). Interestingly, this was not the case for mice with Nr4a1 CRISPR knockdown previously taking cocaine (p= 0.966). Moreover, mice with Nr4a1 CRISPR knockdown previously taking saline did not significantly differ from mice with LacZ control previously taking cocaine (p= 0.878) (**Figure 3p**).

Material and Methods

Animals

Studies were conducted in accordance with guidelines set up by the Institutional Animal Care and Use Committees at University of Maryland School of Medicine. All animals were given food and water ad libitum during the study with the exception of water training. Adult male and female wild-type C57BL/6 mice (University of Maryland Veterinary Resources) and male RiboTag (RT)$^{+/+}$ mice (Rpl22$^{tm1.1Psam/J}$) on a C57Bl/6 background [1] were used. During the entire behavioral study, mice were pair-housed in cages with perforated plexiglass dividers to allow for sensory, but not physical, interaction [2]. Mice were 7 to 8 weeks old at the beginning of the experiments.

Intravenous Cocaine Self-administration

Self-administration experiments involving viral manipulation were conducted in two independent cohorts of animals, at least. Data were then pooled.

Intravenous cocaine self-administration experiments were conducted as described previously [3, 4]. Water-deprived mice were trained to self-administer water (4 days, 2 sessions of 30 min/day) under an FR1 schedule. Following training, animals were anesthetized with ketamine (100 mg/kg) and xylazine (16 mg/kg) and implanted with long-term indwelling jugular catheters (Plastics One, Roanoke, VA). Mice were flushed daily with heparin 50 IU/mL (40%, in saline) and 2.27% Baytril (Bayer, Shawnee, KS; 20%). After 5 days of recovery, mice underwent 10 days of saline or cocaine self-administration under an FR1 schedule (0.5 mg/kg/infusion in saline; 2 hours/day). Responses in the active nosepoke elicited a 10-µl cocaine (or saline) infusion and a 10-s illumination of the active nosepoke light. During this 10-s time out period, nosepokes in the active port were recorded but did not triggered additional infusions. Responses on the inactive nosepoke were also recorded but had no programmed consequences.

To avoid the effect of anesthetic on behavioral and molecular measurements during self-administration experiments, catheter patency was inferred from daily increase in cocaine intake and from psychomotor activation at the end of each session [2]. When unsure, patency was tested with a 30μL intravenous infusion of ketamine (50 mg/kg, in saline). Only mice showing patency were used in data analyses.

Cocaine seeking, Extinction and Drug-induced reinstatement

Twenty-four hours after the last FR1 session, a 1-h seeking test was performed under extinction conditions (i.e., a response resulted in cue presentation but no drug delivery). Following the seeking test, mice were subjected to additional extinction sessions consisting of 5 distinct 1-h sessions separated by 5-min intervals during which animals were placed back in their home cage. Similar to the seeking test, during extinction sessions each response on the active nosepoke resulted in cue presentation but no drug delivery. On the following day, the extinguished mice were injected with cocaine (7.5 mg/kg in saline, ip.) or saline 5 min before a cocaine induced reinstatement test during which each response resulted in cue presentation but no drug delivery [2, 3].

Rap2 activity assay

Rap2 GTPase activity was assessed from whole VP tissue of mice 24 hours after receiving 10 daily cocaine (20mg/kg in saline) or saline intraperitoneal injections. Tissue from 2 mice was pooled per sample and 7 samples were analyzed per condition. Following tissue homogenization, Rap2 activity was measured using a Rap2 activation assay kit following manufacturer's instructions (Cell Biolabs Inc, STA-406-2).

Stereotaxic surgery and viral vectors

Under isoflurane anesthesia, mice were bilaterally injected with viral vectors at the following coordinates: ventral pallidum (from Bregma; 10° angle, anterior/posterior: AP +0.9, medial/lateral: ML ±2.2, dorsal/ventral: DV -5.3), mediodorsal thalamus (from Bregma; 10°

angle, AP: -0.8, ML: ±1.2, DV: -3.7), ventral tegmental area (from Bregma; 7° angle, AP: -3.2, ML: ±1, DV: -4.6), lateral habenula (from Bregma; 10° angle, AP: -1.2, ML: ±0.7, DV: -3.1). Circuit-specific viral expression was achieved using the retrograde properties of adeno-associated virus (AAV) serotype 5: AAV5.hSyn.HI.eGFP-Cre.WPRE.SV40 (Addgene; #105540). Sparse labelling was obtained using Cre-inducible, double inverted open (DIO)-reading frame AAV2-hSyn-DIO-mCherry (Addgene; #50459) diluted to 1.5×10^{11} VP/mL for neuronal morphology [5].

For Nr4a1 overexpression virus, Nr4a1 sequences were obtained from Origene (#MR209316), PCR amplified (Phusion DNA polymerase; New England Biolabs) and cloned into the NheI and NcoI restriction site of the AAV-EF1a-DIO-EYFP vector. The AAV-DIO-Nr4a1-EYFP was packaged into AAV (serotype 9) at UMB Virus Vector Facility. For verification of Nr4a1 overexpression, 300-400 ng of cDNA from VP was synthesized using the reverse transcriptase iScript cDNA synthesis kit (Bio-Rad). mRNA expression changes were measured using qRT-PCR with PerfeCTa SYBR Green FastMix (Quanta). Quantification of mRNA changes was performed using the −ΔΔCT method described previously [4].

Due to the large size of SpCas9 (4.5 kb), which limits its packaging into an AAV, we chose the SaCas9 CRIPSR protein (3.1 kb). By facilitating its packaging into an AAV, its *in-vivo* delivery for genome editing is thus facilitated [6]. Additionally, studies showed that SaCas9 possesses higher cleaving activity over SpCas9 [7]. Moreover, SaCas9 recognizes a 5′-NNGRRT-3′ PAM sequence which is more specific than the SpCas9 PAM sequence. The AAV-CMV-DIO-SaCas9 was packaged into AAV (serotype 9) at UMB Virus Vector Facility. The construct for CRISPR-based knockdown of Nr4a1 was designed by Vector Builder. In brief, exons and splice isoforms of Nr4a1 sequence gene was found on the UCSC genome browser database (http://genome.ucsc.edu/). Based on best transcript alignment, gRNA and PAM sequences were design from the 5' exonic codon with benchling.com. We chose multiplexed sgRNA driven by distinct U6 promoters for an efficient knockdown of the target gene. The following sequences were used for the gRNAs: #1gRNA- ccgtgctcctcagcttgttcc;

#2gRNA- ctctccgaaccgtgacacttc, #3gRNA- caatgcttcgtgtcagcacta. The multiplexed LacZ gene target was used as control construct. eGFP fluorescence protein expression cassette was added in same vector backbone in under CMV promoter (**Supplementary Figure 3c**). For indel assay, VP tissue was injected with a mixture of AAV-CMV-DIO-SaCas9, AAV-Nr4a1-sagRNAx3-CMV-eGFP (or AAV-LacZ-sagRNAx3-CMV-eGFP for control) and AAV.hSyn.HI.eGFP-Cre.WPRE.SV40. After 3-4 weeks, genomic DNA was isolated from each sample using 'QuickExtract DNA Extraction Solution' (LucigenQE0905T). In brief, VP tissue was mixed and vortexed (15 sec) with 400µl of QuickExtract Solution. Tubes were transferred to a heat block for 10 minutes at 65°C and vortexed again for 15 seconds. To deactivate the enzymes, the tube was re-heated at 98°C for 2 minutes. 2µl of the sample were used for PCR using Q5 High-Fidelity DNA Polymerase (NEB #M0494S). PCR amplification surrounding each target site from genomic DNA was performed using the following set of primers: Forw: TGTATTCAAGCTCAATATGG and Rev: AGCTTTCTGCAGCCCTAGAGAG. After confirmation of a single PCR product band on the gel, we purified the PCR product using a PCR purification kit (Qiagen #28106). Set of forward and reverse internal primers were used for sanger sequencing at Genomics Core Facility (Formerly Biopolymer Core Facility) at UMB: Sanger Sequence primers: Forw: AGCAACGAGCCCAGGACC, Rev: GTCCTGCAGGACAGAACCAG. CRISPR indel analysis was performed with ICE (Inference of CRISPR Edits; Synthego) tool from synthego.com using .abi files (LacZ .abi file was used as a control). Our sample was verified for CRISPR indels by various ICE tool indel frequency, or the percentage of the cell population that had insertions or deletions. We further verified CRISPR knockdown efficacy using qRT-PCR: 300-400 ng of cDNA from VP was synthesized as described above and mRNA expression was quantified using the −ΔΔCT method.

RNA sequencing and bioinformatics

Whole ventral pallidum RNA was extracted with the RNeasy Micro kit (Qiagen: 74004; see below for detailed extraction procedure). For RNA sequencing, only samples with RNA

integrity numbers >8 were used. Samples were submitted in biological quadruplicates for RNA sequencing at the UMSOM Institute for Genome Sciences (IGS) and processed as in [1]. Libraries were prepared from 90 ng of RNA from each sample using the NEBNext Ultra kit (New England BioLabs). Samples were sequenced on an Illumina HiSeq 4000 with a 75 bp paired-end read. An average of 86 million reads were obtained for each sample. Reads were aligned to the mouse genome (Mus_musculus. GRCm38) using TopHat2 [8] (version 2.0.8; maximum number of mismatches = 2; segment length = 30; maximum multi-hits per read = 25; maximum intron length = 50,000). The number of reads that aligned to the predicted coding regions was determined using HTSeq [9]. Significant differential expression was assessed using DEseq. RNA-sequencing data are available through the Gene Expression Omnibus database (GEO accession number: TBD) as well as in **Supplementary Table 1**. Gene ontology (GO) functional enrichment analysis was performed on significantly differentially expressed (SDE) genes with Cytoscape software (v. 3.6.1) [10] using the BiNGO plugin [11]. Follow up transcriptional regulator network were obtained with iRegulon [12] by analyzing genes from significant “Cellular Component” GO terms.

RNA extraction and qRT-PCR

RNA extraction and quantitative RT-PCR was performed as previously described [13]. Briefly, ventral pallidum tissue punches were collected 24 h after the last self-administration session or 3 weeks after viral infusion and stored at -80°C. RNA was extracted using Trizol (Invitrogen) and the E.Z.N.A MicroElute Total RNA Kit (R6831-01, Omega) with a DNase step (#79254, Qiagen). RNA quantity was measured using a Nanodrop (Thermo Scientific). Three to four hundred nanograms of complementary DNA was synthesized using a reverse transcriptase complementary DNA synthesis kit (iScript, Bio-Rad). Changes in mRNA expression were measured using quantitative PCR (Biorad) with PerfeCTa SYBR Green FastMix (#95072, Quantabio). Quantification of mRNA changes was performed using the 2–ΔΔCt method, using glyceraldehyde 3-phosphate dehydrogenase (Gapdh) as a housekeeping gene. The list of primers used is available in **Supplementary Table 3**.

Projection-specific mRNA expression

Polyribosome immunoprecipitation was achieved as described in [1, 13]. Briefly, pooled tissue from RiboTag (RT)$^{+/+}$ mice with virally mediated Cre expression in VP → MDT neurons (n= 4-5 mice per sample) was homogenized and 800 µL of the supernatant was incubated in HA-coupled magnetic beads (Invitrogen: 100.03D; Covance: MMS-101R) overnight at 4°C. Magnetic beads were then washed in high salt buffer. Following TRK lysis buffer addition, RNA was extracted with the RNeasy Micro kit (Qiagen: 74004). For input, 50 ng of RNA was used and 1-2 ng of RNA from immunoprecipitated samples were amplified using the Low RNA Input kit (NanoString Technologies®). All samples were then processed with the nCounter Master Kit (NanoString Technologies®) by UMSOM IGS on a custom-made gene expression Code set (see **Supplementary Table 3** for primer sequences). Data were analyzed with nSolver Analysis software as in [1].

In situ *hybridization*

Coronal brain slices (16-18µm) were prepared using a cryostat (Leica) and fluorescent *in situ* hybridization was performed using the RNAscope® kit following manufacturer's instructions (Acdbio, Advanced Cell Diagnosis). Briefly, slide-mounted sections were post-fixed in 10% formalin and dehydrated in ethanol. RNA probes targeting Cre (#312281) and Nr4a1 (#423341-C3) were applied and DAPI staining was used to identify cell nuclei.

Immunohistochemistry

Mice were perfused with 0.1M PBS and 4% paraformaldehyde and brains were post-fixed for 24 h. For dendritic spine morphology and virus placement, 100 µm sections were blocked in 3% normal donkey serum and 0.3% Triton X-100 in PBS for 30 min, then incubated in chicken anti-mCherry (1:500; Novus Biologicals, NBP2 25158) and in rabbit anti-GFP (1:500; Cell Signaling #2555) overnight at 4°C as in [14, 15]. For virus validation a mouse monoclonal

anti-Nr4a1 antibody (1:1000, #sc-365113, Santa Cruz) or a polyclonal rabbit anti-SaCas9 (1:1000; #ab203933, Abcam) were used. Following eight 1 h-PBS washes slices were incubated overnight in anti-chicken-Cy3 (1:1000, Jackson Immuno; #703-165-155) and anti-rabbit-Alexa 488 (1:1000, Jackson Immuno; #111-545-003) or anti-mouse Cy2 (1:1000, Jackson Immuno; #715-225-150), anti-rabbit Cy5 (1:1000, Jackson Immuno; #711-175-152) depending on the condition at 4°C. Finally, following eight 1 h-PBS washes, slices were mounted with Aqua-Poly/Mount (Polysciences) mounting media.

Imaging

RNA puncta counting: Olympus FV500 Confocal Microscope was used to image immunofluorescence. VP image were taken at 40x magnification from 4 sections per animal. Each VP image sample contained 6 stacked images with 1.5µm step. Counting was performed using Image J software (Fiji plugin) [16] by merging all 6 stacked images. Projection-specific cells were identified by the presence of Cre. For colocalization, 300-400 Cre-positive cells were assessed per animal (4 brain sections per mouse) and the proportion of Cre + Nr4a1 double labeling was calculated. For puncta per cell measurements, individual puncta were counted from 120 Cre + Nr4a1 positive cells per mouse. Counting was performed by experimenters blind to the treatment/group conditions.

Dendritic spine counting: Spine images were acquired on a laser-scanning confocal microscope (Leica SP8) with 0.2 µm increments Z-stacks using a 63x objective with 2x digital magnification [1, 14] and quantified with Neuron Studio software (Mt Sinai School of Medicine) [17]. For all morphological analyses, 2–5 cells were averaged per animal. Morphology was blindly assessed.

Statistical analysis

Graphpad Prism 8.4.3. software was used for statistical analysis. Normality was assessed with Bartlett's test. 2-way RM-ANOVAs and 3-way RM-ANOVAs (mixed-effects model) were run with Sidak, and Tukey posthoc tests respectively. Unpaired two-tailed t-tests were used

when appropriate. Samples were excluded if animals did not acquire cocaine self-administration, if not detected (molecular analysis), had inappropriate viral placement, or failed Grubbs' outlier test. No more than 3 animals per group were excluded. Sample sizes were determined from previous studies using self-administration in mice, RNA sequencing, cell-type-specific RNA isolation and neuronal morphology [1, 2, 5]. In figure legends: *$p \leq 0.05$, **$p < 0.01$, ***$p < 0.001$. All graphs represent mean ± s.e.m. Individual values are plotted to report that variation and variance is similar between groups that are compared. Detailed statistics are available in **Supplementary Material 1** and in figure captions of supplementary figures for supplementary data statistics. Data will be made available by the authors upon reasonable request. RNA sequencing data are available through the Gene Expression Omnibus database (GEO accession number: TBD).

References

1. Engeln, M.*, et al.* Individual differences in stereotypy and neuron subtype translatome with TrkB deletion. *Mol Psychiatry* **26**, 1846-1859 (2021).

2. Engeln, M., Fox, M.E. & Lobo, M.K. Housing conditions during self-administration determine motivation for cocaine in mice following chronic social defeat stress. *Psychopharmacology (Berl)* **238**, 41-54 (2021).

3. Engeln, M.*, et al.* Sex-Specific Role for Egr3 in Nucleus Accumbens D2-Medium Spiny Neurons Following Long-Term Abstinence From Cocaine Self-administration. *Biol Psychiatry* **87**, 992-1000 (2020).

4. Chandra, R.*, et al.* Drp1 Mitochondrial Fission in D1 Neurons Mediates Behavioral and Cellular Plasticity during Early Cocaine Abstinence. *Neuron* **96**, 1327-1341 e1326 (2017).

5. Fox, M.E., Figueiredo, A., Menken, M.S. & Lobo, M.K. Dendritic spine density is increased on nucleus accumbens D2 neurons after chronic social defeat. *Sci Rep* **10**, 12393 (2020).

6. Ran, F.A.*, et al.* In vivo genome editing using Staphylococcus aureus Cas9. *Nature* **520**, 186-191 (2015).

7. Xie, H.*, et al.* SaCas9 Requires 5'-NNGRRT-3' PAM for Sufficient Cleavage and Possesses Higher Cleavage Activity than SpCas9 or FnCpf1 in Human Cells. *Biotechnol J* **13**, e1800080 (2018).

8. Kim, D.*, et al.* TopHat2: accurate alignment of transcriptomes in the presence of insertions, deletions and gene fusions. *Genome Biol* **14**, R36 (2013).

9. Anders, S. & Huber, W. Differential expression analysis for sequence count data. *Genome Biol* **11**, R106 (2010).

10. Shannon, P.*, et al.* Cytoscape: a software environment for integrated models of biomolecular interaction networks. *Genome Res* **13**, 2498-2504 (2003).

11. Maere, S., Heymans, K. & Kuiper, M. BiNGO: a Cytoscape plugin to assess overrepresentation of gene ontology categories in biological networks. *Bioinformatics* **21**, 3448-3449 (2005).

12. Janky, R.*, et al.* iRegulon: from a gene list to a gene regulatory network using large motif and track collections. *PLoS Comput Biol* **10**, e1003731 (2014).

13. Chandra, R.*, et al.* A Role for Peroxisome Proliferator-Activated Receptor Gamma Coactivator-1alpha in Nucleus Accumbens Neuron Subtypes in Cocaine Action. *Biol Psychiatry* **81**, 564-572 (2017).

14. Fox, M.E.*, et al.* Dendritic remodeling of D1 neurons by RhoA/Rho-kinase mediates depression-like behavior. *Mol Psychiatry* **25**, 1022-1034 (2020).

15. Francis, T.C.*, et al.* Molecular basis of dendritic atrophy and activity in stress susceptibility. *Mol Psychiatry* **22**, 1512-1519 (2017).

16. Schindelin, J., *et al.* Fiji: an open-source platform for biological-image analysis. *Nat Methods* **9**, 676-682 (2012).

17. Rodriguez, A., Ehlenberger, D.B., Dickstein, D.L., Hof, P.R. & Wearne, S.L. Automated three-dimensional detection and shape classification of dendritic spines from fluorescence microscopy images. *PLoS One* **3**, e1997 (2008).